2022

Multi-Objective Optimization of a Vapor Compression Portable Cooler

Diego Marchi

Vitor Alves

Christian Hermes

Multi-Objective Optimization of a Vapor Compression Portable Cooler

Diego MARCHI [*], Vitor H. F. ALVES, Christian J. L. HERMES

POLO Laboratories, Department of Mechanical Engineering, Federal University of Santa Catarina
Florianópolis, SC, Brazil

[*] Corresponding Author: marchi@polo.ufsc.br

ABSTRACT

This paper presents a multi-objective optimization of a 38-liter vapor compression cooler aiming at performance maximization and weight minimization. An experimental mapping of the thermodynamic efficiencies (internal, external, and overall) of a vapor compression portable cooler running with two different compressors was performed to identify opportunities for energy optimization. In the analysis, the original crankshaft reciprocating compressor was replaced by a small-capacity mini-rotary one with half of the weight and one-third of the shell volume when compared with the baseline one. Albeit the latter presented an overall second-law efficiency about 10% lower, the refrigeration cycle (internal) efficiency increased by 25%, thus indicating not only that the mini-rotary compressor performed better than the original one, but also that there is room for a proper redesign of the heat exchangers. To this end, a steady-state system simulation model was advanced for the design and optimization exercises, which explored not only the evaporator and condenser heat transfer areas, but also the thickness of the cabinet insulating walls. One the one hand, the Pareto front revealed a system configuration that consumes 13% less energy than the baseline cooler if the weight remains unchanged. On the other hand, for the same energy performance, the optimization led to a cooler 15% lighter than the baseline.

1. INTRODUCTION

The market for light portable refrigerators has increased steadily after the introduction of thermoelectric coolers a few decades ago. Nonetheless, such appliances have low energy performance due to their intrinsic thermodynamic irreversibilities (Hermes and Barbosa, 2012). Therefore, compact vapor compression systems emerged as a high-performance alternative, in spite of being much heavier than the thermoelectric devices. Remarkably, the tradeoff between size and efficiency is an essential design aspect of portable coolers (Yee and Hermes, 2019), impelling the industry towards the development of increasingly smaller but efficient compressors (Possamai *et al.*, 2008; Ribeiro, 2012; Lee *et al.*, 2014). Albeit multi-objective optimizations have been carried out for household refrigerators focusing on energy and cost savings (Negrão and Hermes, 2011), from the authors' best knowledge there is no study in the open literature aiming at performance maximization and weight minimization of portable coolers, which is on the focus of the present paper.

To this end, a portable cooler running with two different compressors, namely reciprocating (crankshaft-type) and mini-rotary, were evaluated. First, experimental tests were carried out in order to obtain the key performance parameters for each configuration (*e.g.*, power consumption, cooling capacity, compressor runtime). Since the direct comparison between the overall energy consumption may be unfair from a thermodynamic standpoint, the methodology introduced by Hermes and Barbosa (2012) – consisting of splitting the refrigeration (second law) efficiency into two terms, one associated with internal losses (*e.g.*, friction, mixtures) and another with external losses (*e.g.*, heat transfer across finite temperature difference) – was adopted not only for comparisons purposes, but also to prospect opportunities for further design improvements. In addition, a steady-state simulation model was put forward and validated against experimental data. A multi-objective optimization exercise was carried out for the system running with the mini-rotary compressor, aiming not only at energy performance improvement, but also weight reduction, considering the heat exchangers surface areas as well as the insulation thickness.

2. EXPERIMENTAL WORK

The portable cooler under analysis is illustrated in Fig. 1. The refrigeration system, comprised by a 38-liter cabinet, is equipped with a reciprocating compressor, which runs with 42g of HFC-134a. A fan-supplied tube-fin condenser is responsible to reject the heat to the environment, while the refrigerated compartment is cooled down by a natural draft evaporator distributed along the internal walls. The vapor compression refrigeration loop is depicted in Fig. 2, where one can notice an internal heat exchanger between the capillary tube and the suction line.

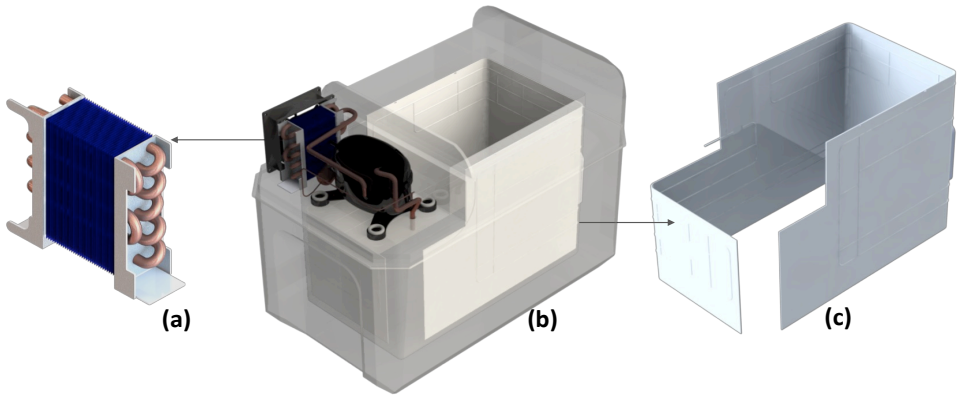

Figure 1: Schematic of the baseline cooler: (a) tube-fin condenser, (b) insulated cabinet and (c) roll-bond evaporator

The characteristics of the compressors considered in this study are described in Table 1. On the one hand, the baseline system has a single-speed reciprocating (crankshaft-type) compressor which operates at 60 Hz. On the other hand, a prospective replacement (also available on the market) is a miniature rotary-type compressor with two compression stages, roughly 50% lighter than the reciprocating one. In general, rotary compressors are usually used in air conditioning applications, as it develops low efficiencies at low evaporating temperatures. Nonetheless, according to manufacturer's data, the mini-rotary compressor can operate in a wide range of evaporating temperatures spanning both fresh-food and freezer conditions. In addition, although it can operate with variable-speed, all the analyses reported in this work were carried out at a fixed speed of 58 Hz, for which the compressor performed the best.

Table 1. Summary of the characteristics of the compressors under analysis.

Compressor	**Reciprocating**	**Mini-rotary**
Evaporating temperature range, °C	-35 to 0	-30 to 20
Compressor EER (LBP), W/W	0.89	1.11
Stroke, cm³	1.3	2.4
Mass, kg	2.3	1.2
Dimensions: *H* | *L* | *W*, mm	159 | 149 | 154	154 | 77 | 107
External shell volume, liter	1.03	0.33
Frequency range, Hz	60	20 to 80

Experimental tests were carried out in a climate chamber with strict control of temperature, humidity and air speed. Temperature at several points in the refrigeration loop were measured using T-type thermocouples with a measurement uncertainty of ±0.2°C. The average air temperature inside the refrigerated compartment was obtained from nine thermocouples, five of which positioned in the horizontal medium plane, as shown in Fig. 3. The thermocouples used for measuring the cabinet air temperatures were brazed in cylindrical copper blocks, following the recommendations of the IEC 62552 (2015) standard. The surrounding air temperature was measured in three different positions around the cabinet (front, right and back). The condensing and evaporating temperatures were evaluated through surface thermocouples placed along the refrigerant piping and compared with the saturation temperature corresponding to the pressure measured by means of strain gauge transducers at the compressor suction and discharge ports. All the surface thermocouples employed a thin electrical insulation medium between the thermocouple and the surfaces to avoid undesired electrical noise.

The instantaneous power consumption was measured during the tests through a digital analyzer with an uncertainty of ±0.1% of the full scale, while the power consumed by other components, such as condenser fan and control board were evaluated beforehand. Figure 4 graphically illustrates the range of tested conditions (30 data points), in a pressure–enthalpy diagram, for both compressors. The numbers stand for the cycle points indicated in Fig. 2.

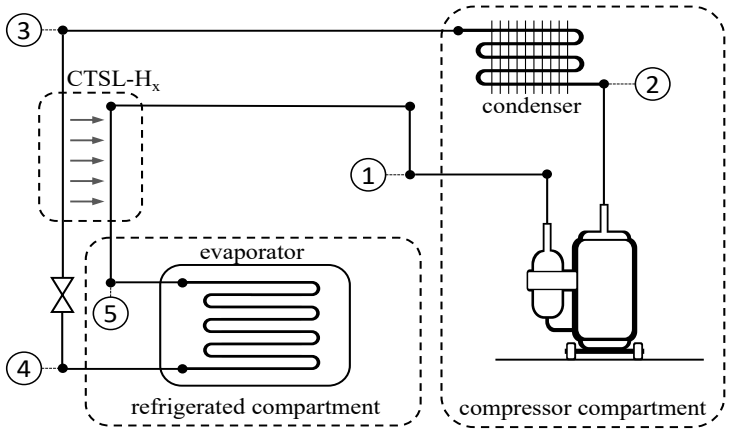

Figure 2: Schematic representation of the refrigeration loop

The overall thermal conductance of the cabinet was estimated based on a reverse heat flux test (Vineyard *et al.*, 1998), according to which the internal temperatures are maintained above surrounding air temperature by means of heat dissipation inside the refrigerated compartment via electric heaters. During the test, the refrigeration system is switched off and the air temperatures inside and outside the cabinet are monitored, along with the power consumed by the heaters. At steady-state condition, the thermal conductance of the cabinet can be calculated from $UA_{cab}=\dot{W}_{res}/(T_i - T_e)$, where UA_{cab} represents the overall cabinet conductance (= 0.52 W/K), $\dot{W}_{res}$ is the mean power dissipated by the heaters, in W, T_i is the cabinet internal temperature and T_e the surrounding air temperature.

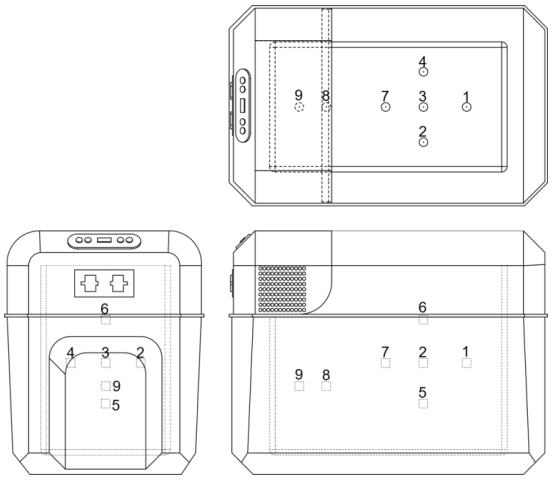

Figure 3: Schematic of cabinet air temperature instrumentation

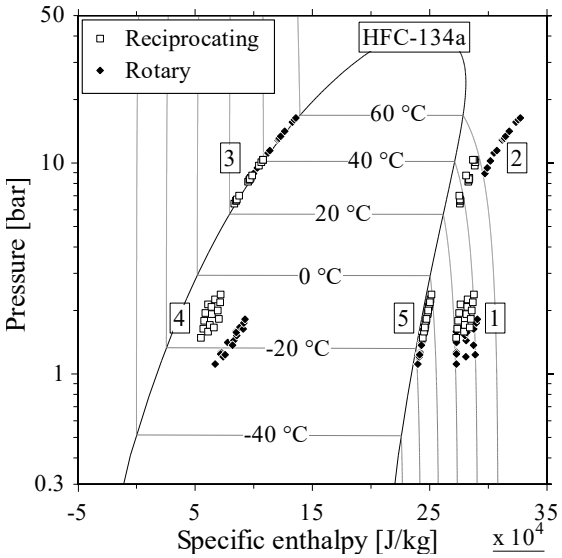

Figure 4: Representation of the whole dataset in a pressure-enthalpy diagram

For the energy consumption tests, electric heaters were installed inside the refrigerated compartment to maintain the storage temperature fixed, which was done by means of a PID controller in such a way that the refrigerator operates at steady-state condition with the compressor running continuously (Hermes *et al.*, 2013). Therefore, the compressor

runtime ratio (*RTR*) can be calculated from $RTR=\dot{Q}_t/\dot{Q}_{ev}$, where $\dot{Q}_t=UA_{cab}(T_e-T_i)$ is the cabinet thermal load whereas $\dot{Q}_{ev}=\dot{Q}_t+\dot{W}_{res}$ is the cooling capacity of the refrigeration system at steady-state conditions, and $\dot{W}_{res}$ is the power dissipated by the heaters. Finally, the energy consumption is obtained from $EC=RTR\sum\dot{W}$, where $\sum\dot{W}$ accounts for the overall power consumption of the system, comprising the compressor, the condenser fan and the control board. For both compressors, the tests were performed under three different surrounding air temperatures (16, 25 and 32°C), and five distinct cabinet internal temperatures (-4, 0, 4, 8 and 12°C), summing up 30 tests in total.

3. THERMODYNAMIC MAPPING

The coefficient of performance of a real refrigeration system is defined by the ratio between the cooling capacity and the overall power consumption (Gosney, 1982):

$$\varepsilon_r = \dot{Q}_{ev} \Big/ \sum \dot{W} \tag{1}$$

The coefficient of performance of an ideal refrigerator running according to the Carnot cycle, where all the thermodynamic processes are reversible, depends only of the cabinet and surrounding air temperatures, where $T_i<T_e$:

$$\varepsilon_{id} = T_i \big/ \left(T_e - T_i\right) \tag{2}$$

Moreover, assuming that the refrigeration system operates ideally between the hot (T_h) and cold (T_c) ends, that stand for the condensing and evaporating temperatures, respectively, the coefficient of performance of an endoreversible (*i. e.,* internally ideal) refrigerator can be calculated as follows:

$$\varepsilon_{ii} = \left(T_i - \Delta T_c\right) \big/ \left(T_e - T_i + \Delta T_h + \Delta T_c\right) \tag{3}$$

where ΔT_h and ΔT_c represent the temperature differences at the hot and cold ends, respectively. It is important to point out that ε_{ii} is the maximum coefficient of performance possible for an ideal refrigeration system running with actual heat exchangers, that is, with a finite temperature difference between the terminals and the reservoirs. It should be noted that once $\Delta T \rightarrow 0$, thus $\varepsilon_{ii} \rightarrow \varepsilon_{id}$.

According to Hermes and Barbosa (2012), the refrigeration efficiency associated with the internal irreversibilities (*e.g.*, friction, mixture) that take place in the refrigeration cycle can be calculated as the ratio between the coefficients of performance of the real and the endoreversible refrigerators, while the thermodynamic efficiency related to the external losses (*e.g.*, heat transfer across finite temperature differences in the condenser and the evaporator) is obtained by dividing the latter by the coefficient of performance of the Carnot refrigeration cycle. Hence, the overall second-law efficiency can be calculated as follows:

$$\eta_{2^{nd}} = \eta_i \eta_e = \left(\varepsilon_r / \varepsilon_{ii}\right)\left(\varepsilon_{ii} / \varepsilon_{id}\right) = \varepsilon_r / \varepsilon_{id} \tag{4}$$

where η_i is the 2nd-law efficiency associated with the cycle internal irreversibilities, whereas η_e is the 2nd-law efficiency associated with the external losses.

Figure 5 shows that the baseline system presented an overall efficiency 22% higher than configurations with the mini-rotary compressor, reflecting the gains in the ε_r as the ε_{id} figures remained fairly constant. On the one hand, the baseline system has higher external efficiencies in comparison to the one operating with the mini-rotary compressor, as the latter presented very high temperature differences in the hot and cold ends. On the other hand, the trends observed for the internal efficiencies are quite the opposite, with the system with the mini-rotary compressor showing better figures than the baseline regardless the working conditions. Actually, this is so as the rotary compressor is notoriously more efficient than the reciprocating one, which is endorsed by the compressor calorimeter EER, as presented in Table 1.

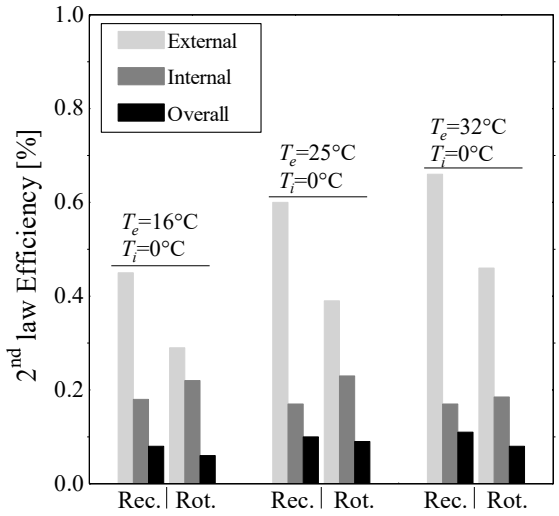

Figure 5: Efficiency deployment: cabinet temperature at 0°C and various surrounding air conditions

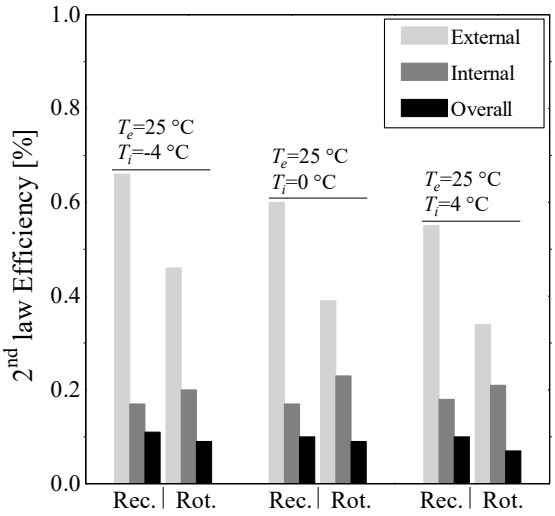

Figure 6: Efficiency deployment: surrounding air temperature at 25°C and various cabinet temperatures

Also, the experimental mapping reveals that a proper sizing of the heat exchangers for operation with the mini-rotary compressor could significantly improve the system performance as its internal efficiency is significantly higher than that observed for the baseline. As the mini-rotary compressor provides higher mass flow rate levels and, consequently, higher heat duties, it requires heat exchangers with larger number of transfer units to work properly.

4. MATHEMATICAL MODELING

A steady-state system simulation model was developed aiming at the optimization exercise, being comprised of the following sub-models for the compressor and the heat exchangers, namely condenser and evaporator, as described below. The formulation followed closely the approach introduced by Gonçalves *et al.* (2008), where the refrigerant charge and capillary tube sub-models were replaced by prescribed evaporator superheating and condenser subcooling, so that the condensing and evaporating temperatures can be calculated respectively from:

$$T_h = T_3 + \Delta T_{sub} \tag{5}$$

$$T_c = T_1 - \Delta T_{sup} \tag{6}$$

This procedure not only eliminates potential convergence issues, but also brings the numerical analysis closer to the design practice, where both the capillary tube and the refrigerant charge are adjusted *posteriori* to guarantee a certain degree of superheating and subcooling.

4.1 Compressor

The compressor sub-model is aimed at determining the displaced mass flow rate ($\dot{m}$), the power consumption ($\dot{W}_k$), and the thermodynamic state of the refrigerant at the compressor discharge based on the working pressures and the refrigerant temperature at the compressor inlet. The mass flow rate and compression power are calculated from:

$$\dot{m} = \eta_v V_{sw} N / v_1 \tag{7}$$

$$\dot{W}_k = \dot{m}\left(h_{2s} - h_1\right)/\eta_g \tag{8}$$

where η_v and η_g stand for the compressor volumetric and global efficiencies, respectively, V_{sw} is the swept volume, N the motor speed, in Hz, and v_1 the specific volume at compressor inlet. Albeit Eqs. (7) and (8) were originally devised for reciprocating compressors (Gosney, 1982), some studies pointed out predictions with acceptable errors when the model is used to calculate power consumption and mass flow rate of rotary compressors (Li, 2013). Based on the heat released by the compressor to the surrounding air, $\dot{Q}_k = UA_k(T_{2s} - T_e)$, where T_e is the surrounding air temperature and

UA_k the compressor thermal conductance, an overall energy balance in the compressor returns the refrigerant state at the outlet:

$$h_2 = h_1 + \left(\dot{W}_k - \dot{Q}_k\right)/\dot{m} \tag{9}$$

The compressor efficiencies were obtained by means of a hot-cycle calorimeter, and correlated as linear functions of pressure ratio (p_{cd}/p_{ev}) and rotational speed (N). The compressor overall thermal conductance (UA_k), in turn, was obtained from tests carried out with the whole system in a climate room.

4.2 Heat exchangers

The refrigerant at the capillary tube outlet can be obtained from the following energy balance:

$$h_4 = h_3 + h_5 - h_1 \tag{10}$$

The compressor inlet temperature (T_1) was calculated from the capillary tube-suction line heat exchanger effectiveness (ε_{ihx}), also adjusted based on experimental data, so that

$$T_1 = T_5 - \varepsilon_{ihx}\left(T_3 - T_5\right) \tag{11}$$

A mean value of 0.8 was obtained from 30 experimental points. Regarding the condenser and evaporator, both thermal models were divided in zones according to the refrigerant thermodynamic state. The former counts with 3 zones (superheated, saturated and subcooled), whilst the latter has two (saturated and superheated) regions. The heat transfer in the saturated zones were calculated considering a constant thermal conductance (UA_{sat}), yielding

$$\dot{Q} = \dot{m}\Delta h = UA_{sat}\Delta T \tag{12}$$

where $\dot{Q}$ stands either for the evaporator cooling capacity or condenser heat duty, in W, and ΔT refers to the respective temperature difference between the refrigerant saturation temperature and thermal reservoir, in K. Concerning the single-phase regions, the heat transfer was calculated from the effectiveness method, as follows:

$$\dot{Q} = \dot{m}\Delta h = \varepsilon_{hx} C_{min} \Delta T_{max} \tag{13}$$

$$\varepsilon_{hx} = 1 - exp(-NTU_{hx}) \tag{14}$$

where ε_{hx} is the temperature effectiveness of the heat exchanger, considered as a function of number of transfer units ($NTU_{hx}=UA_{hx}/C_{min}$), C_{min} is the thermal capacity rate of the stream with the lower figure. The overall thermal conductance terms (UA_{hx}) were all obtained from experimental data obtained for the cooler at steady-state conditions.

5. SIMULATION RESULTS

The simulation model was implemented in the EES platform (Klein, 2011). Figure 7 compares the model predictions for cooling capacity and power consumption with the experimental counterparts, while Fig. 8 does the same for the working pressures. As can be seen, errors within a ±10 % deviation bands were observed for the whole dataset, with just a few outsiders, and roughly 95% of the predictions falling within the ±10% error bounds. Also, a maximum deviation of 2°C between model predictions and experimental data were found for the evaporating and condensing temperatures.

Figures 9 and 10 illustrate the model sensitivity by means of steady-state simulations performed for the refrigeration system operating with the reciprocating and mini-rotary compressor. The performance trends are explored as a function of the runtime ratio, cabinet temperature, and surrounding air temperature, the latter represented as the upper and lower thresholds by the shady bands.

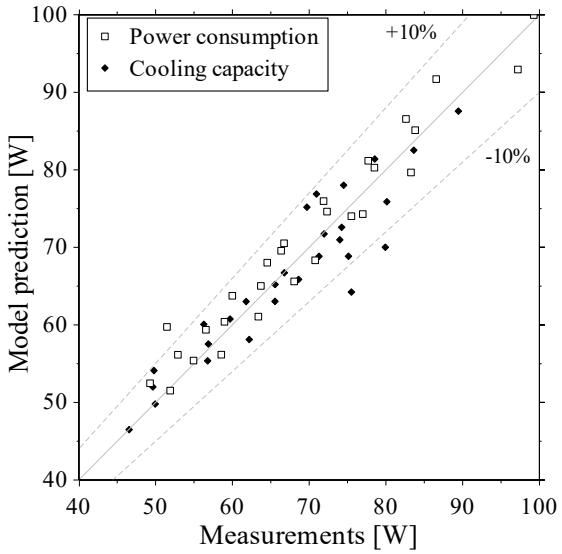

Figure 7: Model validation for the power consumption and cooling capacity

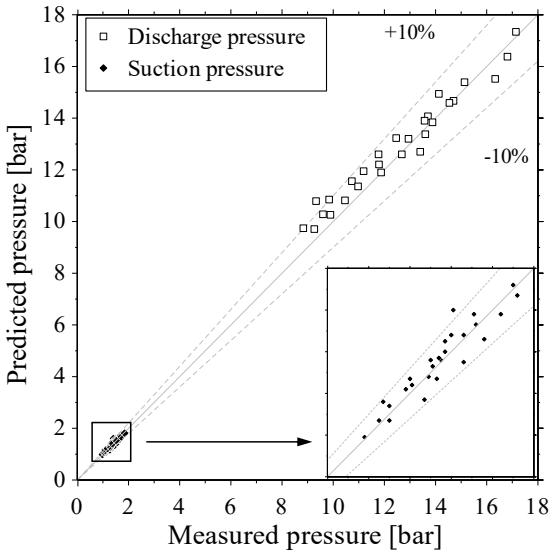

Figure 8: Model validation for the condensing and evaporating pressures

One can notice in Fig. 9 an increasing reduction of the minimum temperature reached for a certain *RTR* when the original compressor is replaced by the mini-rotary one, going from -12 to -30°C when the compressor is kept on continuously (*RTR*=1). Figure 10, in turn, shows that the energy consumption span with regard to the surrounding air temperature is increased by 4 kWh/month in the case the mini-rotary compressor is adopted. Such a greater sensitivity to the ambient temperature variations is another indication that the heat exchangers are undersized for the mini-rotary compressor and shall be properly redesigned.

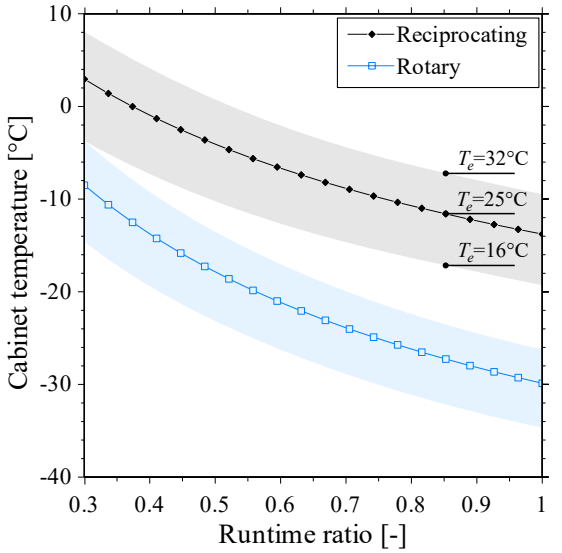

Figure 9: Simulation results for the cabinet air temperature as a function of the compressor *RTR*

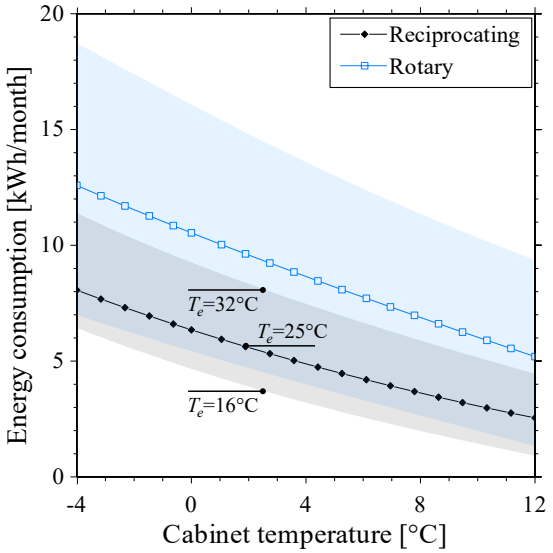

Figure 10: Simulation results for energy consumption as a function of the cabinet air temperature, T_i

6. OPTIMIZATION SCHEME

In compact coolers, besides energy, a reduction of the total mass is also compelling, particularly for off-grid applications, where portability is a must and battery power supply is employed. Moreover, the thermodynamic

mapping exercise indicated a large margin for energy consumption reduction once the heat exchangers are undersized. Therefore, an optimization exercise was conducted not only to resize the condenser and the evaporator to run with the mini-rotary compressor, but also to find out the optimal heat exchanger areas and cabinet walls insulation thickness that lead to minimum energy consumption for a fixed weight, or minimum weight for a fixed energy consumption.

6.1 Problem parametrization

In order to verify the trade-off between mass and energy consumption, the most relevant system components were evaluated and putted into account according to the objective function:

$$w_t = w_{cd} + w_{ev} + w_{ins} + w_{rest} \tag{15}$$

where w stands for the mass, and the subscripts *cd*, *ev*, *ins,* and *rest* refer to the condenser, evaporator, insulation and other components, respectively, with the latter representing the mass of the plastic structure, fan, pipelines, etc. The original system mass when employing the mini-rotary compressor was 10.2 kg, as summarized in Table 2.

Table 2. Mass distribution in the original system mounted with the mini-rotary compressor

Component	Condenser	Evaporator	Insulation	Other	Compressor	TOTAL
Mass, kg	0.29	1.38	0.96	6.37	1.2	10.2
Distribution, %	2.9	13.5	9.4	62.5	11.8	100

The thermal effect of the following independent variables, namely condenser heat transfer area, A_{cd}, evaporator heat transfer area, A_{ev}, and insulating wall thickness, δ_{ins}, were explored in the optimization exercise. Therefore, for the heat exchangers, the overall heat transfer coefficients (U) were held constant, with the area influencing the heat transfer rate. Similarly, in order to consider the thermal effect of the insulation thickness on cabinet overall conductance, the inner cabinet volume was kept constant while the wall thickness was changed. The condenser mass was modeled as a linear function of A_{cd}, fixing the properties of the heat transfer surface (*e.g.* compactness factor, Colburn j-factor) and changing only the heat exchanger length, so that $w_{cd}=0.841+0.061A_{cd}$. The evaporator mass, which consists basically of a flat plate, was calculated straightforwardly from $w_{ev}=\rho_{al}\delta_p A_{ev}$, where ρ_{al} is the aluminum density, δ_p the plate thickness (1.5 mm). The mass of the insulated walls was calculated from $w_{ins}=\rho_{pu}\delta_{ins}(LW+LH+WH)+\rho_{pu}\delta_{ins}^2(L+W+H)+\rho_{pu}\delta_{ins}^3$, where ρ_{pu} is density of the PU insulating foam and δ_{ins} is the insulation thickness. For the optimization exercise, the surrounding and cabinet air temperatures were prescribed at 25 and -4 °C, respectively.

6.2 Optimization results

The analysis was firstly conducted to find out the set of parameters (A_{cd}, A_{ev}) that minimize the total mass for a fixed energy consumption. In this case, the insulation thickness was not changed, which would be the first choice on industrial grounds since the cabinet modifications may involve serious production investments. To this end, the built-in EES *conjugate directions method* was employed (Klein, 2011). The results can be seen in Pareto front depicted in Fig. 11 (the line with open bullets), pointing out the loci of minimum mass for each energy consumption. On the one hand, changing the evaporator and condenser areas by +161% and -27%, respectively, a reduction of 17% in energy consumption is verified. On the other hand, if one keeps the energy consumption constant, the total mass of the system can be reduced 5% by decreasing the evaporator area by 50% and increasing the condenser area by 74%.

Later, the insulation thickness was also explored along with the heat exchangers areas. The Pareto front considering a variable insulation thickness can be seen also in Figure 11 (the line with solid bullets). In this case, the results were even more expressive, showing an energy consumption reduction of 28% for the original mass, and reducing the mass in 6% maintaining the energy consumption. The former requests an increase of 63% in the condenser area, a reduction of 55% in the evaporator area, and an addition of 24 mm in the insulation thickness, while the latter is achieved when the evaporator area is reduced by 64%, the condenser area increased by 28% and 9.5 mm of PU insulation is added to the walls. The maximum mass reduction achieved, also considering the compressor replacement, was 15% (1.7 kg). Finally, Fig. 12 presents an energy consumption reduction map considering the original mass (10.2 kg) under different operating conditions. A variation of ~6.5% is verified within the analyzed envelope, indicating that the improvements provided by the optimization exercise remain fairly constant regardless the operating condition.

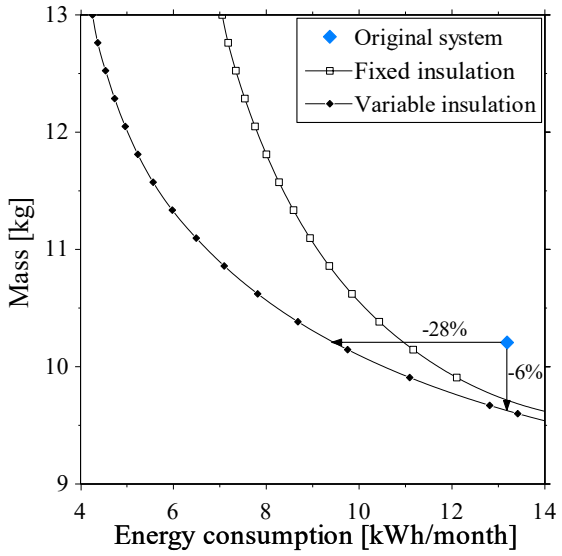

Figure 11: Optimum mass as a function of energy consumption for a fixed operating condition

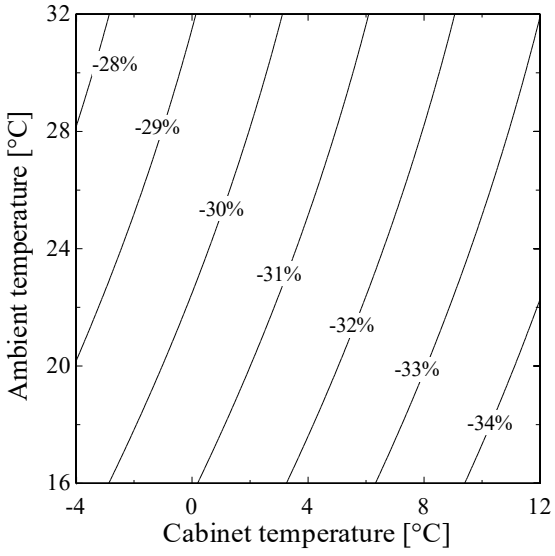

Figure 12: Maximum energy savings for all operating conditions holding the original mass fixed

7. FINAL REMARKS

A methodology for the thermodynamic comparison of a compact cooler running with a reciprocating and a mini-rotary compressor was employed. Experimental tests were conducted at three levels of surrounding air temperature (16, 25 and 32°C) and at five levels of cabinet temperature (-4, 0, 4, 8 and 12°C) in a climate chamber. The operating parameters of each configuration were accounted to quantify the internal and external irreversibilities of the refrigeration system. The baseline configuration showed higher efficiency values, roughly 20% higher than those observed for the system running with the mini-rotary compressor. Albeit the external efficiencies with the mini-rotary compressor presented lower figures than the baseline, the internal efficiency showed values slightly higher than the baseline, thus indicating that a proper heat exchanger sizing is a must for compressor replacement. From this standpoint, an optimization exercise was conducted to verify the effect of the heat exchangers areas and the insulation thickness on both energy consumption and total weight. Taking the original system equipped with the mini-rotary compressor as a reference, the optimization showed that it is possible to reduce the energy consumption by 28% while maintaining the original weight, or to reduce 6% of the total weight when keeping the energy consumption fixed. Comparing the final (optimized) system for the mini-rotary compressor with the baseline (equipped with the original reciprocating compressor), the total mass was reduced from 11.3 to 9.6 kg for a fixed energy consumption (15%), and the energy consumption was reduced from 10.8 to 9.4 kWh/month for a fixed weight (13%). Finally, since a cost structure can be correlated with the mass of the commodities, specifically for the heat exchangers, this methodology can be extended to a combined cost/energy/mass minimization exercise, which has great interest on industrial grounds.

NOMENCLATURE

Roman

A	area (m²)	UA	thermal conductance (W/K)
h	specific enthalpy (J/kg)	v	specific volume (m³/kg)
H	height (m)	V	volume (m³)
L	length (m)	w	mass (kg)
$\dot{m}$	mass flow rate (kg/s)	W	width (m)
N	compressor speed (Hz)	$\dot{W}$	power (W)
NTU	number of transfer units (-)		
p	pressure (bar)		
$\dot{Q}$	heat transfer rate (W)		
T	temperature (°C)		

Greek		*hx*	heat exchanger
δ	thickness (mm)	*i*	internal
ε	1st-law efficiency (-)	*id*	ideal
η	2nd-law efficiency (-)	*ins*	insulation
ρ	density (kg/m³)	*k*	compressor
		p	plate
Subscript		*pu*	polyurethane
al	aluminum	*r*	real
cab	cabinet	*res*	electric heater
c	cold end	*sat*	saturation
cd	condenser(ing)	*sub*	subcooling
e	external	*sup*	superheating
ev	evaporator(ing)	*sw*	swept
h	hot end	*tot*	total

REFERENCES

Gonçalves, J. M., Melo, C., Hermes, C. J. L (2009) A semi-empirical model for steady-state simulation of household refrigerators, App. Therm. Eng. 29, 1622–1630

Gosney, W. B. (1982) Principles of refrigeration, Cambridge University Press, Cambridge, UK.

Hermes, C. J. L., Barbosa, J. R. (2012) Thermodynamic comparison of Peltier, Stirling, and vapor compression portable coolers, Applied Energy 91, 51–58

Hermes, C. J. L., Melo, C., Knabben, F. T. (2013) Alternative test method to assess the energy performance of frost-free refrigerating appliances, App. Therm. Eng. 50, 1029–1034

IEC62552 (2015). Household refrigerating appliances – Characteristics and test methods – Part 1: General requirements (Standard 62552), International Electrotechnical Commission, Geneva, Switzerland.

Klein, S. A. (2011) Engineering Equation Solver User's Manual, F-Chart Software, Middleton-WI, USA

Lee, J., Lee, U., Chung, J., Lee, U. (2014). Development of a Miniature Twin Rotary Compressor, Int. Refrigeration and Air Conditioning Conference at Purdue, West Lafayette, IN, USA

Li, W. (2013) Simplified steady-state modeling for variable speed compressor, App. Therm. Eng. 50, 318–326

Negrão, C. O. R., Hermes, C. J. L. (2011). Energy and cost savings in household refrigerating appliances: A simulation-based design approach. App. Energy 88(9), 3051–3060.

Possamai, F., Lilie, D. E. B., Zimmermann, A. J. P., Mongia, R. (2008) Miniature Vapor Compression System, Int. Refrigeration and Air Conditioning Conference at Purdue, July 14-17, West Lafayette, IN, USA

Ribeiro, G. B. (2012) Development and analysis of a compact cooling system using the microcompressor, 13th InterSociety Conf. Thermal and Thermomechanical Phenomena in Electronic Systems, IEEE, San Diego, CA, USA

Vineyard, E.A., Therese, K.S., Kenneth, E.W., Kenneth, W.C. (1998) Superinsulation in refrigerators and freezers, ASHRAE Trans. 104, 1126-1134

Yee, R. P., Hermes, C. J. L. (2019) Thermodynamic design of a mesoscale vapor compression refrigeration device, App. Therm. Eng. 147, 509-520

ACKNOWLEDGEMENT

This study was conducted under the auspices of the Brazilian Government INCT (CNPq 404023/2019-3, FAPESC 2019TR0846) and EMBRAPII (PPOL-1901.0020) funding programs.